Ultrasonic enhancement of the acidity, surface area and free fatty acids esterification catalytic activity of sulphated ZrO2-TiO2 systems

Ultrasonic enhancement of the acidity, surface area and free fatty acids esterification catalytic activity of sulphated ZrO_2-TiO_2 systems

D.C. Boffito[a], V. Crocellà[b], C. Pirola[a], B. Neppolian[c, d] , G. Cerrato[b], , M. Ashokkumar[d], C.L. Bianchi[a]

[a]Università degli Studi di Milano – Dipartimento di Chimica, via Golgi 19, 20133 Milano, Italy

telephone: 0039 02 503 14293, fax: 0039 02 503 14300

[b]Università di Torino – Dipartimento di Chimica Inorganica, Chimica Fisica e dei Materiali, via P. Giuria 7, 10125 Torino, Italy

[c]SRM Research Institute, SRM University , Kattankulathur, Chennai, India

[d]The University of Melbourne – School of Chemistry, Melbourne, Parkville 3052, Australia

Abstract

Different samples of sulphated zirconia and mixed zirconia/ titania (SO_4^{2-}/ZrO_2 and $SO_4^{2-}/80\%ZrO_2$-$20\%TiO_2$), were prepared with traditional and ultrasound (US) assisted sol-gel synthesis and tested in the free fatty acids esterification. The catalysts were characterized through acid sites quantification by ion exchange, specific surface area and porosity measurements (N_2 adsorption at 77 K), XRD, XPS and FT-IR spectroscopy. SEM-EDX and TEM analyses were also used to investigate the morphology of the samples. The results of this study demonstrate the possibility of increasing the acidity and the surface area of sulphated zirconia through the addition of TiO_2 and tune the same properties with the continuous or pulsed US. It is also demonstrated that it is necessary to combine specific values of both acidity and surface area and which type of active sites are essential to obtain better catalytic performances in the free fatty acids esterification.

Keywords: ultrasonication, sol-gel, sulphated zirconia, sulphated titania, acid catalysts, heterogeneous catalysis, esterification, free fatty acids

1. Introduction

Biodiesel is becoming increasingly important as an alternative fuel for diesel engines as a consequence of the diminishment of petroleum reserves and as part of the effort to save the global environment.

Biodiesel is the biofuel obtained from the biomass derived from lipid feedstock. The most common process used to convert lipids, i.e. triglycerides, into biodiesel is the transesterification reaction [1, 2]. Transesterification is a process where triglycerides contained in vegetable oils or animal fats react with an alcohol, usually methanol, yielding fatty acid methyl esters (FAME) and glycerol in presence of an alkaline catalyst [3]. The main problem posed by the use of alkaline catalysts is represented by the obligation of using feedstock with very low acidity (< 0.5% wt). In fact, free fatty acids (FFA) contained in raw oils give saponification problems as a consequence of their reaction with the alkaline catalyst ($RCOOH + NaOH \rightarrow RCOONa + H_2O$). The presence of soaps during the transesterification hinders the contact between reagents and makes difficult the separation of the products. Refined, low acidity oilseeds may be easily converted into biodiesel, but their employment not only significantly raises the production costs, but also increases food and water demands [1]. It is so highly desirable to produce biodiesel from specifically selected non-edible cultures or from low-cost feedstock such as used cooking oils and animal fats [2, 4, 5]. The main issue posed by such raw materials is the need of standardization, especially with regard to the decrease of the acidity, so to avoid saponification reactions. In fact, crude oils and not refined greases in general, are characterized by very high acidities, ranging from 3 to 40 wt% [6].

In recent years a great deal of attention has been focused on the study of the pre-esterification as a method to lower the acidity of the raw oils to be used for biodiesel production [5, 7-10]. The esterification reaction of FFA also allows to improve the final yield in biodiesel as the obtained products are FAME, i.e. biodiesel, as represented in the Scheme 1. The esterification reaction can be performed using both homogeneous [11, 12] and heterogeneous catalysis [13, 14]. For liquid phase reactions, the latter approach is preferred as it brings benefits such as the easier separation of the catalyst from the products, thus facilitating catalyst recovery and re-use. Much attention has been focused on the use of ion exchange acid resins as catalysts for the FFA esterification reaction [5, 7-10]. A significant outcome of these studies lies in the correlation between the catalytic activity of the tested catalysts with the acidity present on the catalyst outer surface regardless of the nature of adopted catalysts [10].

As an alternative to the ion exchange resins inorganic acid catalysts, such as zirconium sulphate and sulphated zirconia, can be used. These materials are active because of the presence at the surface of both Brønsted acidic centers and Lewis acid sites (*i.e.* coordinatively unsaturated (*cus*) Zr^{4+} cations), as evidenced by Morterra et al. [15]. Zirconium sulphate has been widely studied for the FFA esterification reaction [10, 16] due to its high activity. Sulphated zirconia is widely studied for other different kinds of reactions, such as isomerizations, alkylations and esterification of other carboxylic acids [18], but its use for FFA esterification directly performed in the oil is reported in few studies [17].

In the present work, mixed zirconium and titanium sulphated oxides (SO_4^{2-}/80%ZrO_2-20%TiO_2) are reported as potential catalysts for the FFA esterification reaction to be performed directly in the crude oil to be used for biodiesel production. The results of this study demonstrate the possibility of increasing the surface acidity of the catalysts with the addition of TiO_2 to the ZrO_2 and the use of US during the catalysts synthesis. The effect of different power intensities and the use of pulsed US are also investigated. The beneficial effects of acoustic cavitation on catalysts properties are already clearly reported in some recent papers [19-21]. It has also been shown in

the current study how it is possible to modulate catalysts features, such as the acidity and the surface area, employing different experimental conditions during the US-assisted synthesis.

2. Experimental

2.1 Catalysts preparation

All the catalysts were synthesized using the sol-gel method. SO_4^{2-}/ZrO_2 (hereafter referred to as SZ) was synthesized using traditional sol-gel method, while $SO_4^{2-}/80\%ZrO_2$-$20\%TiO_2$ (hereafter referred to as SZT) was synthesized using both traditional and US-assisted sol-gel techniques. Zirconium tetra-n-propoxide (ZTNP) and titanium tetra-iso-propoxide (TTIP) were used as precursors in all the cases. i-PrOH was used as a solvent in all the synthesis with a molar ratio to the precursors (ZTNP+TTIP) equal to 15 [18, 19]. Molar ratio between water and the alkoxides (ZTNP+TTIP) was kept constant at 30 as already reported elsewhere [18] in the traditional syntheses and varied in the ones with US. $(NH_4)_2SO_4$ was used as sulphating agent, keeping the molar ratio SO_4/Zr or SO_4/Zr+Ti constant at 0.15 in all the cases [18].

Nitric acid was used to promote the hydrolysis of the precursors, as already reported in other works from the authors [18, 19]. The molar ratio HNO_3/Zr or HNO_3/Zr+Ti was kept constant at 0.21 [18].

A list of all the samples along with different synthesis parameters is provided in Table 1. Samples termed USZT refer to US-obtained sulphated $80\%ZrO_2$-$20\%TiO_2$. The name is followed by the US power, by the length of US pulses and by the molar ratio of water over precursors, as reported in Table 1. For example, USZT_40_0.1 _30 indicates a sample $SO_4^{2-}/80\%ZrO_2$-$20\%TiO_2$ obtained with US, using the 40% of the maximum power, with US on for 0.1 seconds (pulse length) and off for 0.9 seconds, using a water/ZTNP+TTIP molar ratio equal to 30.

ZTNP 70% in 1-PrOH, TTIP 98%, i-PrOH, HNO_3 69.5% wt and $(NH_4)_2SO_4$ were used and are all Fluka products.

In the case of traditional sol-gel method, the starting solution was prepared by mixing 1.23 ml of TTIP and 5.52 ml of ZTNP with 25 mL of the solvent (i-PrOH) for 30 minutes in a bath thermostated at 298 K, stirring at 300 rpm through a mechanical stirrer. The aqueous solution containing the sulphating agent and HNO_3 was then added to the mixture at the rate of 0.25 ml/min. After finishing the addition, the gel was left aging for additional 90 minutes under stirring.

In the case of US synthesis, a 20 kHz horn sonicator was used. The tip of the horn was placed inside the sol-gel mixture in a 100-mL water-jacketed reactor. The power was varied at 20 and 40% of amplitude of the maximum power (450 W). Also US pulses were adopted for some syntheses.

For what concerns the US syntheses, as in the case of the traditional synthesis, the starting solutions were prepared by mixing the precursors with the solvent and stirring them for 30 minutes. After the mixing, the solutions were thermostated at 298 K and the aqueous solution containing the sulphating agent and HNO_3 was added at the rate of 0.25 ml/min. After finishing the addition of the aqueous solution, the gel was left aging for additional 10 minutes under US irradiation.

The total synthesis time reported in Table 1 indicates the time required to perform the whole sol-gel process, while the sonication time indicates the fraction of the total synthesis time while US were functioning. As an example, consider entry 4 in Table 1. The total synthesis time is 43’0’’, which is the sum of the time required for the addition of the aqueous solution to one of the precursors at a rate of 0.25 ml/min and 10 minutes for the aging. Since the US was powered in pulse mode with on/off ratio 9:1, the actual sonication time is given by (1/10) • 43’’0’, i.e. 4’18’’.

The temperature was monitored during the course of the ultrasonic synthetic experiments. The temperature increased up to 313 K during the first few minutes of the reaction, then remained constant till the end of the experiments.

All the samples were calcined in static air atmosphere at 773 K for 3 hours with a heating rate of 2.5 K/min. The choice of such a temperature, along with the choice of both slow heating rate and duration of the treatment, was dictated by the need to preserve the largest number of sulphate groups after the calcination, as suggested by Dijs *et al*. [17].

In order to demonstrate that the choice of specific calcination conditions is fundamental to avoid the loss of a too large fraction of surface sulphates groups, thereby affecting the catalytic activity, the sample SZT was also calcined at 773 K for 6 hours, employing the same heating rate. This sample is reported as SZT_773_6h in entry 2a, Table 1.

2.2 Catalysts characterization

Nitrogen adsorption – desorption isotherms were measured at 77 K using a Micromeritics Tristar 3000 system. All samples were degassed at 433 K overnight on a vacuum line. The standard multi-points Brunauer–Emmett–Teller (BET) method was utilized to calculate the specific surface area (SSA). The pores size distributions of the materials were derived from the adsorption branches of the isotherms based on the Barett–Joyner–Halenda (BJH) model [22].

XPS analyses were obtained using an M-probe apparatus (Surface Science Instruments). XP spectra were collected using a VG ESCALAB 220i-XL spectrometer equipped with a monochromatic Al Kα X-ray source which emitted a photon energy of 1486.6 eV at 10 kV and 12 mA. The measurements were processed at a step size either 1 eV (wide scans) or 0.1 eV (region scans). Film samples were screwed down to Al holders. Precursor samples were adhered to the surface of In metal and then mounted on Al holder. Charging of catalyst samples was corrected by setting the binding energy of adventitious carbon (C 1s) at 284.6 eV. Curve fitting and quantification of XP spectra were performed using Eclipse and Casa XPS programs.

FTIR spectra were run at 4 cm^{-1} resolution with a Bruker IFS 113v spectrophotometer equipped with MCT detector. The powder samples were investigated in the form of thin layer depositions (~ 10 mg cm^{-2}) on a pure Si wafer, starting from aqueous suspensions of the powders. After drying, all samples were activated in controlled atmosphere at 623 K in a homemade IR quartz cell, equipped with KBr windows, connected to a conventional vacuum glass line capable of a residual pressure $<1 \times 10^{-5}$ Torr, which allowed to perform strictly in situ adsorption/desorption experiments of molecular probes. The study of surface acidity was performed using as probe 2,6-dimethylpyridine (2,6-DMP; Lu). The standard IR experiment of 2,6-DMP adsorption/desorption on the various samples, was carried out as follows: (i) admission in the IR cell of an excess dose of 2,6-DMP vapour (~ 2 Torr), and equilibration at beam temperature (hereafter BT), i.e., the temperature reached by samples in the IR beam, for 5 minutes; (ii) evacuation of the base excess at BT for 15 minutes; (iii) desorption of the strongly bonded 2,6-DMP fraction was eventually carried out at 423 K for 15 minutes.

The quantification of the Brønsted acidity was carried out through ion exchange with a of NaCl saturated solution, leaving it in contact with the catalysts for 30 hours [23]. The evaluation of H^+ concentration was carried out using a pH-meter. The number of H^+ milliequivalents released per gram of catalyst was then calculated.

The crystalline nature of the samples was investigated by X-ray diffraction (XRD) using a PW3050/60 X'Pert PRO MPD diffractometer from PANalytical working Bragg-Brentano, using as source the high power ceramic tube PW3373/10 LFF with a Cu anode equipped with Ni filter to attenuate Kβ. Scattered photons have been collected by a RTMS (Real Time Multiple Strip) X'celerator detector.

The morphology of the catalysts was inspected by means of high resolution electron transmission microscopy (HR-TEM) and scanning electron microscopy (SEM). SEM-EDX (Energy-dispersive X-ray spectroscopy) was used to determine the amount of Zr, Ti and S in the samples.

TEM images were recorded using a JEOL 3010-UHR instrument (acceleration potential: 300kV; LaB_6 filament). Samples were "dry" dispersed on lacey carbon Cu grids. Philips XL-30CP with RBS detector of back scattered electrons was used for SEM-EDX analyses.

Sulphates amount of both SZT and SZT_773_6h samples was determined by ion chromatography (Metrohm mod. 883 Basic IC Plus) so to assess the loss of sulphate groups generated by the different calcination procedures. The solutions injected in the ion chromatograph and containing the sulphates were obtained suspending the catalysts in a NaOH solution 0.1 M at ambient temperature and then filtering the liquid through a 0.45 μm PTFE filter, as already reported elsewhere [24].

2.3 Catalytic tests

All catalysts were tested in the FFA esterification reaction with methanol.

The selected feedstock was a commercial rapeseed oil (initial acidity 0.1% wt), acidified with oleic acid up to 7.5% wt, in order to obtain a high initial acidity. The stoichiometric alcohol/acid ratio for the esterification reaction is 1:1, but it is advisable to use a higher amount of alcohol to shift the reaction towards the desired products. For this reason, the added amount of methanol was calculated taking into account the oil mass to treat and not the reaction stoichiometry. Consequently, the methanol/oil weight ratio was 16:100, corresponding to about 4.5:1 MeOH:oil molar ratio. All catalytic tests were performed with the catalyst suspended in the reaction medium, using 25-mL magnetically stirred vials as esterification reactors. Therefore, the composition of each vial was: 17 g of oil at 7.5% wt of acidity, 2.7 g of methanol and ~0.064 g of catalyst, corresponding to the 5% of catalyst over FFA by weight.

The reactors were thermostated before starting the activity tests using an oil bath at 336 ± 2 K. The mechanical stirring was maintained at 300 rpm. All the activity tests were carried out for 6 hours.

Oil acidity was determined through titration analyses with KOH 0.1 M in ethanol. Since oil and KOH are not soluble, each sample was dissolved before titration in a mixture of diethylether: ethanol 9:1 per volume, in order to obtain a homogeneous mixture. Phenolphthalein was used as indicator. The percentage of FFA content per weight was calculated as in Eq.1 [5, 25, 26].

$$FFA = \frac{V \times MW \times C}{W} \times 100 \qquad \text{Eq. 1}$$

where V is the volume of KOH solution employed for titration (mL), MW is the molecular weight of oleic acid (282.46 mg $mmol^{-1}$), C is the concentration of KOH (mmol mL^{-1}) and W is the weight of the analyzed sample (mg).

FFA conversions, *i.e.* the percentage of oleic acid converted in oleic methylester were determined as in Eq. 2.

$$FFAconv. = \frac{a_i - a_f}{a_i} \times 100 \qquad \text{Eq. 2}$$

where a_i is the initial acid concentration by weight and a_f is the acid concentration after 6 hours of reaction.

All the products used for catalytic tests are Fluka products of high purity.

As already evidenced in previous studies of the authors [5, 7], the experiment carried out in absence of the catalyst showed no FFA conversion.

3. Results and Discussion

3.1 Catalysts characterization

3.1.1 Structural and morphological features

Brønsted acidity (measured through ion exchange), specific surface area and porosity features of all samples are reported in Table 2.

It can be noticed that the simple addition of TiO_2 to the sulphated ZrO_2 increases the acidity of the catalyst more than 2.5 times (compare entries 1 and 2 in Table 2). It is reported in the literature that the addition of TiO_2 to ZrO_2 can increase the surface concentration of –OH groups [27, 28]. This behaviour is generally observed for mixed oxides and it is probably due to the charge imbalance resulting from the heteroatoms linkage for the generation of acid centres [29]. The addition of TiO_2 to ZrO_2 is also reported to decrease the particle size and increase the surface area [30] as observed for the samples synthesized in the current study.

It has been observed that with the use of US during the synthesis a further increase in acidity occurred, as well as the surface area (compare entries 1 and 2 with entries from 3 to 12 in Table 2).

The improvement in the properties of the catalysts is probably due to the effects generated by acoustic cavitation. Acoustic cavitation is the growth of bubble nuclei followed by the implosive collapse of bubbles in solution as a consequence of the applied sound field. This collapse generates transient hot-spots with local temperatures and pressures of several thousand K and hundreds of atmospheres, respectively [31]. Very high speed jets (up to 100 m/s) are also formed. As documented by Suslick & Doktycz [21], in the presence of an extended surface, such as the surface of a catalyst, the formation of the bubbles occurs at the liquid-solid interface and, as a consequence of their implosion, the high speed jets are directed towards the surface. The use of sonication in the synthesis of catalysts can therefore result in the enhancement of the distribution of the active phase on the support [20], increasing the rates of intercalation by a variety of species into a range of chalcogenides solids, improving the nucleation production rate (*i.e.* sol-gel reaction production rate) and the production of surface defects and deformations with the formation of brittle powders [21].

At equal water/precursors molar ratios, the acidity of the catalysts increases further when pulse-on time of higher than 0.3 are adopted (compare entries 5, 8, 10 with entry 12 in Table 2). For these catalysts an increase in the SSA, as well as in the acidity is observed if compared to the sample obtained with continuous US.

An attempt was made to explain the effect of various pulse lengths and on/off ratios in terms of two times, τ_1 and τ_2 characteristics of each cavitation system [21, 32]. τ_1 is the time required to produce and then grow chemically active gas bubbles, τ_2 is the time taken by all the gas bubbles generated during the previous US pulse to dissolve away. If τ_1 is shorter than the US pulse length, the system activates. If τ_2 is longer than the interval time from one US pulse to the following one, gas bubbles still present in the system can generate bubble nuclei able to grown within the following US pulse. Hence, the active bubbles population is high at short τ_1 with long τ_2. This condition is more easily achieved when long pulse lengths and short intervals between one US pulse to the other are adopted. During the US pulse bubbles also coalesce leading to "degassing effect". Moreover, at long US pulses with short intervals, including continuous sonication, degassing may result in a lower number of active bubbles: it can be stated that there is an optimal on/off ratio for US pulse times for which maximum cavitation efficiency (maximum number of active bubbles) can be achieved.

Considering the effect of different water/precursors ratios, a general observation can be done: the SSA decreases when higher water amounts are used (compare entries from 6 to 9 and 11 to 12 in Table 2). This may be ascribed to a decrease of US power per unit volume inside the sol-gel reactor. Increasing and decreasing the water amount can be seen in fact as increasing and decreasing, respectively, the reactor size [19]. When the ultrasonic power per unit volume is increased as a consequence of the diminishment of the reactor size, higher energy is supplied to the system. That is the reason why a lower water amount might lead to a higher surface damage and, as a consequence, to the formation of extra surface area under the effect of US. The effect of the increase of water amount on the SSA is particularly evident for the sample USZT_40_0.5_60, i.e., the one obtained with the highest H_2O/precursors ratio (entry 9 in Table 2). For this catalyst, the SSA is in fact significantly lower than the ones of the samples obtained with lower H_2O/ZTNP+TTIP ratios. From the BJH adsorption data (data not provided for the sake of brevity), it is evident that all the samples are characterized by similar pore size distribution. In particular, the distribution resulted to be rather narrow and mainly located in the

lower region of the mesopores. In Table 2 the average pore diameter and the volume of the pores are reported for all the catalysts. No significant differences in the pores dimensions were observed among the samples.

For what concerns how the water/precursors ratio affects the catalysts acidity, it appears that increasing it up to a certain amount brings to an increase in the H^+ concentration (compare entries from 6 to 9 and 11 to 12 in Table 2). In fact, the rate of the hydrolysis, *i.e.*, the rate of the sol-gel process, is enhanced when using higher water amounts. Moreover, the higher the water amount in the sol-gel medium, the higher the probability that H_2O molecules can be chemically bounded producing extra $–OH^+$ Brønsted acidity. Nevertheless, increasing the water/precursors ratio over a certain amount (30 for pulsed and 15 for continuous US, entries 8 and 11 in Table 2, respectively), seems to have a negative effect on the acidity concentration. In fact, the risk of the extraction of acid groups by the excess of water increases as well. In addition, a role might have been also played by the different power densities, which lead to a more or less effective surface damage, as already explained for the differences in the specific surface areas.

For the same reason, the increase of the water amount produces a lowering of the overall Brønsted acidity and not just the decrease of the SSA for the sample USZT_40_0.5_60, (entry 9 in Table 2). As a consequence, these results may be considered due to the same phenomenon.

The XRD analysis highlights the total absence of crystalline structure in all materials. Curve (1) in Figure 1 (SZT sample) is typical of an amorphous system. For the sake of brevity, we reported only this diffractogram, as all the others are almost perfectly coincident. The XRD pattern of SZT_773_6h is also reported in Figure 1 [see curve (2)]. In this case, the material exhibits a net crystalline structure, revealing a series of reflections consistent with the presence of both ZrO_2 and TiO_2, in tetragonal and anatase phase, respectively. This result highlights the effects of the different calcination times (3 vs. 6 hours) at the same temperature (773 K): it is evident that these conditions deeply affect the nature of the above materials.

HR-TEM and SEM investigations of all samples further confirm what XRD analysis indicated. HR-TEM images (reported in Figure 2) show the almost total amorphous nature of the particles

in all cases: for the sake of brevity, we decided to report the features of SZT as this is typical of all systems (see the left hand image). On the contrary, crystalline particles with irregular shape (average diameter in the 4-7 nm range and exhibiting net fringe patterns) are easily observable in the case of the SZT_773_6h material (see the right hand image). SEM images are not reported here as the useful information about the morphology of the samples are already given in Figure 2 for the HR-TEM survey.

The results of ion chromatography obtained for the samples SZT and SZT_773_6h are reported in Table 3. Sulphates concentration evaluated for these two systems indicates that the sample calcined for long time (SZT_773_6h) significantly loses part of its surface sulphates groups, thus resulting in SO_4^{2-} content that is 20% less than SZT.

After all these preliminary characterization measurements, it can be stated that the choice of the calcination conditions reported in the catalysts preparation section (3 hours at 773 K) allows to obtain materials that still possess a good amount of surface sulphate groups. In fact, though the increase of the calcination time and/or the employment of a higher calcination temperature, would permit to generate crystalline materials, the subsequent consistent loss of surface sulphates might produce a drastic decrease of the catalytic activity.

3.1.2. Spectroscopic measurements

The region O 1s of the XP spectra are reported in Figure 3 for the samples SZ, SZT and USZT_40_1_30. XP spectra of the other samples obtained with US are not reported, being these almost perfectly coincident with the one reported for USZT_40_1_30.

In the XP spectra no significant amount of impurities was observed except for the ubiquitous carbon contaminant. In the case of the latter element, only the C 1s peak at 284.6 eV (due to –CH– species) was present. The spectrum of S 2p (not reported for the sake of brevity) was never intense, due to the low intrinsic sensitivity factor of this element, and could be fitted for all the samples by a single component at BE = 169.3 eV, in agreement with that expected for sulphur in sulphates [33] and consistent with previous results relative to other SZ samples [18, 34-36].

No appreciable presence of S-containing species with valence different from S^{+6} was ever observed. As for the S/Zr atomic ratios, they are reported in the Table 4 as well as the other atomic ratios between the elements. For the sample USZT_40_1_30 the calculated ratio of S/Zr+Ti is higher than the two samples obtained without ultrasound, i.e. 0.54 (USZT_40_1_30) vs. 0.40 (SZT) and 0.32 (SZ). The higher content of S in SZT than SZ can be explained considering that Ti is more electronegative than Zr. Therefore, the formation of mixed Zr and Ti species might have increased the electropositive character of Zr, thereby stabilizing sulphate groups, as also reported by Das et al. [28]. A higher amount of superficial sulphur indicates a higher surface functionalization. This may more likely result in a higher catalytic activity.

The data obtained by XPS are in all cases far larger than those obtained by EDX (reported in Table 2). This is in agreement with the prevalent surface localization of sulfates introduced by impregnation [36]. The sulphation of zirconia samples, yielding strong acidic properties, has been reported to modify the spectral features of both O 1s and Zr 3d XPS signals [34-38]. But, unlike what has been tried by other authors [37, 38] the intrinsic complexity of the O 1s spectral region, brought about by the presence of several O-containing components, does not favor meaningful quantitative analytical use of the XPS O 1s peak. The peak of the Zr 3d doublet was found to be in any case regular with BE values (182.2–184.6 eV) for all the samples (spectra not reported for the sake of brevity), consistent with literature data relative to Zr(IV) species in the oxide phase [33-36].

The FTIR spectra, in the 4000-800 cm^{-1} range, were collected for all samples after activation at 623 K in O_2 atmosphere. They showed the typical spectral features of sulphate-modified zirconia. These systems have been widely studied in recent years by means of FTIR spectroscopy [39-45] and, therefore, these spectra have not been presented.

IR spectroscopic investigation of 2,6-DMP (Lu) adsorption/desorption is a useful analytical tool in surface chemistry because: (i) the strong base can interact, in a molecular form, with both weak and strong Lewis acid site [15, 45]. The presence of methyl groups in the two α-positions

of the heteroaromatic ring renders labile and reversible at BT, or just above that, the species adsorbed on weaker Lewis sites, whereas the species adsorbed on strong Lewis sites are much less labile and can thus be resolved; (ii) the interaction with acid protonic sites (Brønsted acid centers) yields lutidinium ions (LuH^+), whose spectral features can be easily recognized and differentiated from those of all other 2,6-DMP adsorbed species [15, 45].

Figure 4 reports, for some of the systems of interest, the main analytical spectral features in the region of the 8a–8b ring vibrational modes of adsorbed (solid lines) and desorbed (broken lines) 2,6-DMP at BT. When a large dose of 2,6-DMP is adsorbed, a band doublet at $\nu > 1615$ cm^{-1} (namely, ~1645 and ~1627 cm^{-1}) appears for all systems. This spectral feature clearly reveals the presence of abundant and strongly held LuH^+ species [15, 44], indicative of the presence of surface Brønsted acid centers.

As for the signals observed in the range below 1615 cm^{-1}, on the basis of literature data [15, 44], they can be ascribed as follows:

(i) A strong band at 1580 cm^{-1} is due to the 8b mode of all 2,6-DMP species adsorbed in a molecular form (liquidlike physisorbed species and H-bonded species).

(ii) A second strong component located at 1592 cm^{-1} is ascribed to the partner 8a mode of 2,6-DMP H-bonded to surface OH groups.

(iii) A third higher-υ band, present as a weak shoulder at 1606 cm^{-1} only in the case of the USZT_40_1_30 sample, can be ascribed to 2,6-DMP interacting with medium-strong Lewis acid sites [coordinatively unsaturated (*cus*) Zr^{4+} or Ti^{4+} cations]. The presence of this component in one single sample indicates that, only specific synthesis conditions (*i.e.*, using 40% of the US maximum power, continuous US, and a water/precursors molar ratio equal to 30) are able to generate at the surface of the material the above mentioned sites.

When excess base is removed by vacuum at BT (see dotted lines in Figure 4), the bands due to protonated 2,6-DMP either remain virtually unchanged or slightly increase (meaning that the Brønsted-bound species are strongly adsorbed). On the contrary, the overall intensity of the

envelope at $\upsilon < 1610$ cm^{-1} decreases drastically, as expected of H-bonded and/or physisorbed species. Within this envelope, only in the case of the USZT_40_1_30 sample, part of the 8a band of Lewis-coordinated 2,6_DMP remains at 1608 cm^{-1}, together with a residual fraction of the 8b band at 1580 cm^{-1}, indicating the presence of a stronger fraction of Lewis acid sites. After evacuation at 423 K (these spectra are not shown in order to not overload the figure) only the signals at $\upsilon > 1610$ cm^{-1} remain with virtually unchanged intensity (confirming that Brønsted-bound species are very strongly held), whereas no spectral components are present at lower frequencies yet, meaning that all the other species are desorbed during this mild treatment.

The results of the elemental analysis obtained by the SEM-EDX analysis are displayed in Table 2. It can be observed that the ratio between Zr and Ti corresponds to that used in the synthesis mixtures. Differently, the amount of sulphur, indicated as S/(Zr+Ti) atomic ratio in Table 2, varies for the different samples and, in some cases, it is far from the adopted 0.15. Indeed, it can be noticed that some samples, i.e. USZT_40_0.5_15 (entry 7), USZT_40_1_15 (entry 11) and USZT_40_1_30 (entry 12) exhibit an higher sulphur on the surface, mainly ascribable to the different synthesis conditions adopted.

3.2. Catalytic tests

The results of the catalytic tests are shown in Figures 5 and 6. In Figure 5 the FFA conversions (%) obtained at the end of the reaction (6 hours) are reported for the samples synthesized using the same H_2O/precursors ratio, whereas in Figure 6 the conversions of the catalysts obtained using different H_2O/precursors ratio are shown. A typical trend of the FFA conversion over time is represented in Figure 7 for the sample USZT_40_1_30 as way of example.

In Figure 5 it can be observed that both the addition of TiO_2 to the SO_4^{2-}/ZrO_2 system and the use of US in specific conditions during the synthesis are able to improve the catalytic performances. As can be observed in Figure 5, the addition of TiO_2 alone is able to improve the activity of the catalysts in the FFA esterification. The addition of TiO_2, in fact, as already

highlighted in the discussion concerning the results of the characterization of the catalysts, is able to increase the Brønsted acidity and, as a consequence, the catalytic activity (compare entries 1 and 2 in Table 2).

Moreover, the SZT sample calcined for long time (SZT_773_6h) exhibits almost no catalytic activity (results not reported for the sake of brevity). This catalytic behaviour might be ascribable to the loss of part of the sulphates occurred during the calcinations step. This hypothesis is also confirmed by the sulphates concentration evaluated by ion chromatography and whose results are reported in Table 3. The SZT_773_6h sample is characterized by a lower sulphates concentration and, as a consequence, by a lower acid capacity (see Table 2) than the "plain" SZT sample (calcined for only 3 hours). Considering the samples obtained with the US pulses with on/off ratio from 0.3/0.7 on, the conversion does not increase much more if compared to the one achieved with the sample obtained via traditional sol-gel synthesis . Their conversions are in fact comparable (see samples USZ_40_0.3_30, USZ_40_0.5_30, USZ_40_0.7_30 and SZT in Figure 5). The similarity in the catalytic performance of these catalysts may be ascribable to the fact that they are characterized by comparable values of SSA (entries 2, 5, 8, 10 in Table 2) and, in the case of the catalysts obtained with pulses, also by comparable acidities (entries 5, 8, 10 in Table 2). A high SSA may in fact be disadvantageous for the catalysis of the reaction here studied. FFA are highly sterically hindered molecules, which might not be able to penetrate inside the pores as narrow as those of the catalysts here synthesized. The importance of the location of the active sites on the outer surface of the catalyst has already been evidenced by the authors in a previous work for other kinds of materials [7]. Therefore, it is possible to assume that, in the present case, the active sites located on the catalyst's outer surface are the most responsible for the reaction to occur. For high SSA, it is more likely that most part of the active sites is located inside the catalyst particles and, therefore, is not exploited in the catalytic process. As a consequence, for these samples, the high surface area results in a low catalytic performance.

The best catalytic performance is reached by the sample USZT_40_1_30, *i.e.* the one obtained using continuous US at higher power. This catalyst results in fact in a doubled catalytic activity with respect to the samples prepared either with the traditional synthesis or with the use of pulsed US. In spite the acidity of this catalyst is lower than that of the samples obtained with the US pulses, it is characterized by a rather low surface area (entry 12 in Table 2) that can be associated with a localization of the active sites mainly on its outer surface. This feature results in many active sites immediately available for an efficient catalysis. As previously evidenced by the FTIR measurements, it is also important to highlight, that only in the case of the USZT_40_1_30 sample, a not negligible number of medium-strong Lewis acid sites is present at the surface, together with a high number of strong Brønsted acid centers. The good catalytic performances of this catalyst show that the presence of both these active sites is a necessary condition in order to obtain reasonably high values of conversion. As already evidenced by some of the authors, the acid-catalyzed esterification reaction may occur at the surface of catalyst on both Brønsted acidic centers and Lewis acid sites (*i.e.* coordinatively unsaturated (*cus*) Zr^{4+} cations) [18].

The low catalytic activity of the sample USZT_20_1_30 may be ascribable to the US power, probably not sufficient to activate the sol-gel reaction under the effect of the cavitation. In the case of the sample USZT_40_0.1_30, the unsatisfactory catalytic activity might be due to the too low on/off pulses ratio. Too short pulse times may in fact not be sufficient to initiate the acoustic cavitation in the medium, as previously explained and as evidenced in literature [21, 32].

In Figure 6, a comparison among the catalytic activity of the samples obtained with continuous US and with the use of 0.5 on/off pulses are displayed for different water/precursors ratios.

As it can be noticed, there is a remarkable difference between the samples USZT_40_1_15 and USZT_40_1_30, *i.e.* obtained using continuous US. On the contrary, the same difference is not evident in the case of the corresponding catalysts obtained with pulsed US, i.e. USZT_40_0.5_15 and USZT_40_0.5_30. This catalytic behaviour can be explained

considering that USZT_40_1_15 and USZT_40_1_30 possess distinct surface and morphological properties, resulting in different catalytic performances, whereas the samples, USZT_40_0.5_15 and USZT_40_0.5_30 are characterized by similar values of acidities and SSA, showing very close values of conversion. It can be noticed that the SSA of USZT_40_1_15 is considerably higher than the SSA of the catalyst obtained in the same conditions but doubling the amount of water (USZT_40_1_30). This latter catalyst, as reported above, results to be the best catalyst in the FFA esterification reaction.

In Figure 8 the FFA conversions as a function of the concentration of the acid sites normalized to the surface area are reported for the most significative samples. It can be observed that the best catalyst, i.e. USZT_40_1_30, possesses the highest ratio of acid sites over surface area. This catalyst results in the highest FFA conversions among all the other samples, in spite it is not characterized by the highest acidity. This confirms that FFA esterification occurs mainly on the active sites located on the outer face of the catalysts. The sample SZT_773_6h exhibits almost no conversion and shows the lowest content of acid sites/m^2. Samples SZT, USZT_40_0.3_30, USZT_40_0.5_30, USZT_40_0.7_30 exhibit very similar FFA conversion as well as similar concentration of meqH^+/m^2. The sample SZ is characterized by a lower meqH^+/m^2 ratio and shows a lower catalytic activity than the above cited samples, with the exception of SZT_773_6h. This result confirms the importance of the localization of an high number of active acid sites on the outer surface of the catalyst for the reaction here studied. In the present work an high number of active acid sites on the outer surface of the catalyst was achieved adopting continuous ultrasound in the sol-gel synthesis of the sulphated ZrO_2-TiO_2 systems.

FFA conversion results may appear discouraging from a first approach, in particular if compared to the other results reported in literature for similar catalysts [28]. Nevertheless, it has to be taken into account that these catalysts are normally tested for the esterification of shorter chain carboxylic acids [18, 46, 47] and that, also in the case of the FFA esterification, they are usually experimented in the pure substrate, *i.e.* as pure fatty acid [28], and not directly in the

acid oil. Taking into account these considerations, the FFA conversions obtained in this work appear encouraging.

Moreover, the outcome of this study is particularly important for what concerns the possibility of tuning the properties of acid catalysts based on mixed oxides by means of US (continuous or pulsed). This might be interesting also in view of the application of sulphated zirconias in other kinds of reactions, such as isomerizations, alkylations and esterifications of other kinds of carboxylic acids.

4. Conclusions

This study demonstrates how the surface acidity and specific surface area of sulphated zirconia can be increased by both adding TiO_2 and using ultrasound (US) in precise experimental conditions to assist the sol-gel synthesis of the catalysts.

The beneficial effects of the use of US in the sol-gel synthesis of the SO_4^{2-}/ZrO_2-TiO_2 systems are ascribable to the occurrence of acoustic cavitation, which causes faster hydrolysis (sol-gel reaction) rates and surface damage. This effect is particularly evident for the catalysts obtained with the use of pulses longer than 0.3 seconds. For these catalysts the acidity significantly increases along with the specific surface area if compared to the ones obtained with shorter pulses.

The more efficient catalyst in the FFA esterification reaction resulted to be the one obtained with continuous US and higher powers. For this sample, in fact, the lower surface area allows the location of the active acid sites mainly on the outer surface of the catalysts. In this way, the FFA molecules can undergo a faster catalytic transformation. Moreover, it has been demonstrated that this catalyst is the only one that possesses both Lewis and Brønsted acidity. Therefore, its good catalytic performances can be ascribed to the presence of both these active sites, together with a low value of SSA.

Acknowledgements

The authors are grateful to the Australian Government (Department of Education, Employment and Workplace Relations) for awarding the Endeavour Research Fellowship of the Australian Awards to Dr. Daria C. Boffito.

References

[1] E. Lotero, Y. Liu, D.E. Lopez, K. Suwannakara, D.A. Bruce, J.G. Goodwin, Ind. Eng. Chem. Res. 44 (2005) 5353.

[2] M. Canakci, H. Sanli, J. Ind. Microbiol. Biotechnol. 35 (2008) 431.

[3] M.W. Formo, J. Am. Oil Chem. Soc. 31 (1954) 548.

[4] Y. Zhang, M.A. Dube, D.D. McLean, M. Kates, Bioresour. Technol. 89 (2003) 1.

[5] C.L. Bianchi, D.C. Boffito, C. Pirola, V. Ragaini, Catal. Lett. 134 (2010) 179.

[6] A. Srivastava, R. Prasad, Renew. Sustain En. Rev. 4 (2000) 111.

[7] C. Pirola, C. L. Bianchi, D. C. Boffito, G. Carvoli, V. Ragaini, Ind. Eng. Chem. Res. 49 (2010) 4601

[8] C. Pirola, D.C. Boffito, G. Carvoli, A. Di Fronzo, V. Ragaini, C.L. Bianchi, in: D. Krezhova (Eds.), Recent Trends for Enhancing the Diversity and Quality of Soybean Products, Intech, 2011, p. 321, http://www.intechopen.com/books/recent-trends-for-enhancing-the-diversity-and-quality-of-soybean-products/soybean-oil-de-acidification-as-a-first-step-towards-biodiesel-production.

[9] C.L. Bianchi, C. Pirola, D.C. Boffito, A. Di Fronzo, G. Carvoli, D. Barnabè, R. Bucchi, A. Rispoli, in: M. Stoytcheva and G. Montero (Eds.) Biodiesel Feedstocks and Processing Technologies, Intech, 2011, p. 3, http://www.intechopen.com/books/biodiesel-feedstocks-and-processing-technologies/non-edible-oils-raw-materials-for-sustainable-biodiesel.

[10] D.C. Boffito, C. Pirola, C.L. Bianchi, Chem. Today 30 (2012) 42.

[11] D.A. Aranda, R.T. Santos, N.C. tapanes, A.L. Dantas, O.A. Antunes, Catal. Lett.122 (2008), 20.

[12] J.M. Marchetti, A.F. Errazu, Biomass. and Bioenergy, 32 (2008), 892.

[13] M. Di Serio, M. Cozzolino, M. Giordano, R. Tesser, P. Patrono, E. Santacesaria, Ind. Eng. Chem. Res., 46 (2007) 6379.

[14] J.M. Marchetti, V.U. Miguel, A.F. Errazu, Fuel, 86 (2007) 906.

[15] C. Morterra, G. Cerrato, G. Meligrana, Langmuir, 17 (2001) 7053.

[16] J.C. Juan, J. Zhang, M.A. Yarmo, Appl. Cat. A 332 (2007) 209.

[17] I.J. Dijs, J.W. Geus, L.W. Jenneskens, J. Phys. Chem. B 107 (2003) 13403.

[18] S. Ardizzone, C.L. Bianchi, G. Cappelletti, F. Porta, J. Catal. 227 (2004) 470.

[19] B. Neppolian, Q. Wang, H. Yamashita, H. Choi, Appl. Catal. A 333 (2007) 264.

[20] C. Pirola, C.L. Bianchi, A. Di Michele, P. Diodati, D. Boffito, V. Ragaini, Ultrason. Sonochem. 17 (2010) 610.

[21] K.S. Suslick, S.J. Doktycz, Effects in: T.J. Mason (Eds.), Advances in Sonochemistry, Jai Press, London, 1990, p. 197.

[22] S.J. Gregg, K.S.W. Sing, Adsorption, Surface Area and Porosity, Acad. Press, London, 1982.

[23] D. E. López, J.G. Goodwin Jr., D. A. Bruce, J. Catal. 345 (2007) 381.

[24] C. Sarzanini, G. Sacchero, F. Pinna, G. Cerrato, C. Morterra, J. Mater. Chem. 5 (1995) 353.

[25] B. M. E. Russbueldt, W. F. Hoelderich, Appl. Catal. A 362 (2009) 47.

[26] S. Pasias, N. Barakos, C. Alexopoulos, Chem. Eng. Technol. 29 (2006) 1365.

[27] B. Neppolian, Q. Wang, H. Jung, H. Choi, Ultrason. Sonochem. 15 (2008) 649.

[28] D. Das, H.K. Mishra, N.C. Pradhan, A.K. Dalai, K.M. Parida, Microp. Mesop. Mat. 80 (2002) 327

[29] T. Kataoka, J.A. Dumesic, J. Catal. 112 (1988) 66.

[30] X. Fu, L.A. Clark, Q. Yang, M.A. Anderson, Environ. Sci. Technol. 30 (1996) 647.

[31] C. Sehgal, R.P. Steer, R.G. Sutherland, R.E. Verrall, J. Chem. Phys. 70 (1979) 2242.

[32] A. Henglein, R. Ulrich, J. Lilie, J. Am. Chem. Soc, 111 (1989) 1974.

[33] J. F. Moulder, W. F. Stickle and K. D. Bomben, Handbook of X-rayPhotoelectron Spectroscopy, Perkin Elmer, Eden Praire, 1992.

[34] S. Ardizzone, C.L. Bianchi, Appl. Surf. Sci., 152 (1999) 63.

[35] S. Ardizzone,C.L. Bianchi, Surf. Interface Anal., 30 (2000) 77.

[36] C. Morterra, G. Cerrato, S. Ardizzone, C.L. Bianchi, M. Signoretto, F. Pinna, Phys. Chem. Chem. Phys., 4 (2002) 3136.

[37] Z. Paal, U. Wild, M. Muhler, J.-M. Manoli, C. Potvin, T. Buchholz, S. Sprenger G. Resofski, Appl. Catal. A, 188 (1999) 257.

[38] T. Buchholz, U. Wild, M. Muhler, G. Resofski, Z. Paal, Appl. Catal. A, 189 (1999) 225.

[39] M. Bensitel, O. Saur, J.C. Lavalley, G. Mabilon, Mat. Chem. Phys. 17 (1987) 249.

[40] F.R. Chen, G. Coudurier, J.F. Joly., J.C. Vedrine, J. Catal. 143 (1993) 616

[41] R.A. Comelli, C.R. Vera, J.M. Parera, J. Catal. 151 (1995) 961.

[42] C. Morterra, G. Cerrato, M. Signoretto, Catal. Lett. 41 (1996) 101.

[43] C. Morterra, G. Cerrato, F. Pinna, M. Signoretto, J. Phys. Chem. 98 (1994) 12373.

[44] C. Morterra, G. Cerrato, S. Di Ciero, Appl. Surf. Sci. 126 (1998) 107.

[45] C. Morterra, G. Meligrana, G. Cerrato, V. Solinas, E. Rombi, M.F. Sini, Langmuir 19 (2003), 5344.

[46] J.C. Juan, Y. Jiang, X. Meng, W. Cao, M.A. Yarmo, J. Zhang, Mat. Res. Bullettin 42 (2007) 1278.

[47] S. Ardizzone, C.L. Bianchi, G. Cappelletti, R. Annunziata, G. Cerrato, C. Morterra, P. Scardi, Appl. Cat. A 360 (2009) 137.

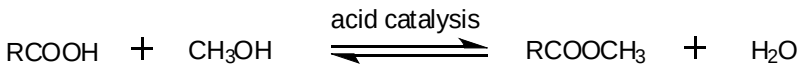

Scheme 1: Esterification reaction of a carboxylic acid with methanol.

Entry	**Sample**	**Composition**	**US power (% max power)**	**Pulses (on/off)**	**H_2O: prec. mol ratio**	**Synthesis time**	**Sonication time**
1	SZ	SO_4^{2-}/ZrO_2	-	-	30	123'0''	0''
2	SZT	$SO_4^{2-}/80\%ZrO_2$-20%TiO_2	-	-		123'0''	0''
2a	SZT_ 773_6h		-	-		123'0''	0''
3	USZT_20_1_30		20	1		43'0''	43'0''
4	USZT_40_0.1 _30		40	0.1/0.9		43'0''	4'18''
5	USZT_40_0.3_30			0.3/0.7		43'0''	12'54''
6	USZT_40_0.5_7.5			0.5/0.5	7.5	17'30''	8'45''
7	USZT_40_0.5_15				15	26'0''	13'0''
8	USZT_40_0.5_30				30	43'0''	21'30''
9	USZT_40_0.5_60				60	77'0''	38'30''
10	USZT_40_0.7_30			0.7/0.3	30	43'0''	30'6''
11	USZT_40_1_15			1	15	26'0''	26'0''
12	USZT_40_1_30				30	43'0''	43'0''

Table 1. List of all samples and of employed synthesis parameters (max. power = 450 W).

Entry	Catalyst	Acid capacity (meq H^+/g)	SSA (m^2g^{-1})	V_p (cm^3g^{-1})	Ave. BJH D_p (nm)	Zr:Ti weight ratio	S/(Zr+Ti) atomic ratio
1	SZ	0.30	107	0.20	6.0	100	0.090
2	SZT	0.79	152	0.19	5.0	79:21	0.085
2a	SZT_773_6h	0.21	131	0.20	5.0	n.d.	n.d
3	USZT_20_1_30	0.92	41.7	0.12	12.5	80:20	0.095
4	USZT_40_0.1_30	1.03	47.9	0.11	9.5	81:19	0.067
5	USZT_40_0.3_30	1.99	232	0.27	4.5	81:19	0.11
6	USZT_40_0.5_7.5	1.70	210	0.20	5.0	78:22	0.086
7	USZT_40_0.5_15	2.02	220	0.20	5.0	80:20	0.13
8	USZT_40_0.5_30	2.17	153	0.20	5.0	78:22	0.12
9	USZT_40_0.5_60	0.36	28.1	0.10	10	79:21	0.092
10	USZT_40_0.7_30	1.86	151	0.16	5.0	78:22	0.11
11	USZT_40_1_15	3.06	211	0.09	7.0	80:20	0.15
12	USZT_40_1_30	1.56	44.1	0.09	7.0	80:20	0.17

[a]Not determined

Table 2. Acid capacities (ion exchange), specific surface areas (BET) and porosity features (Pores volume V_p and average diameter D_p), elemental composition (EDX) of all catalysts.

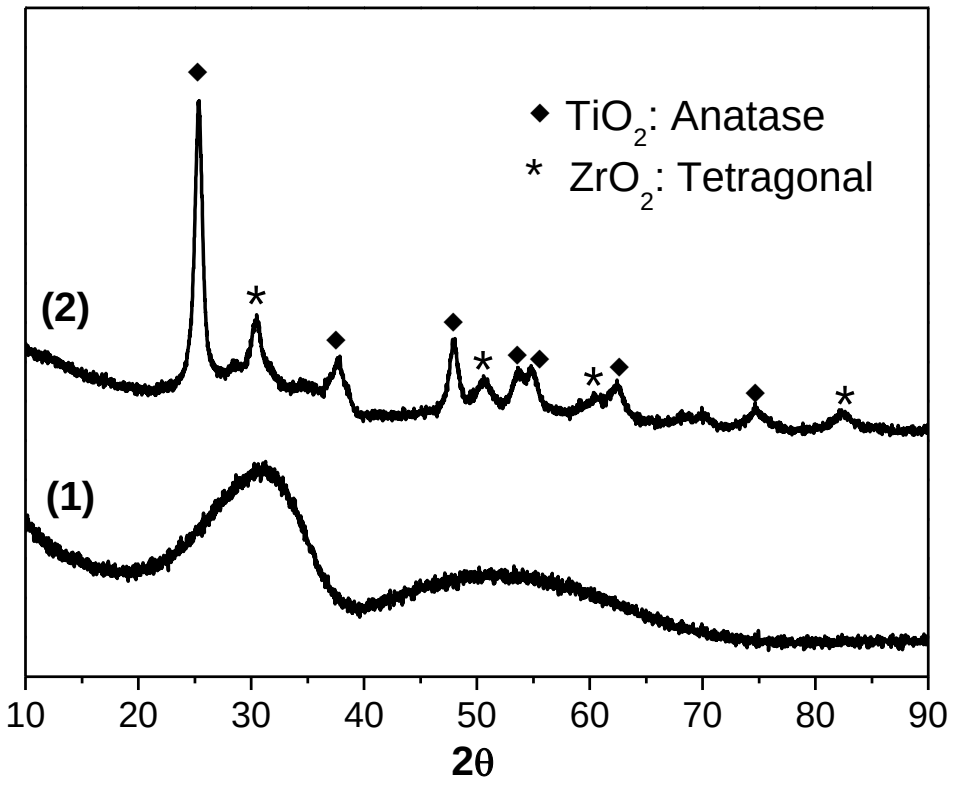

Figure 1: XRD patterns of SZT (1) and SZT_773_6h (2).

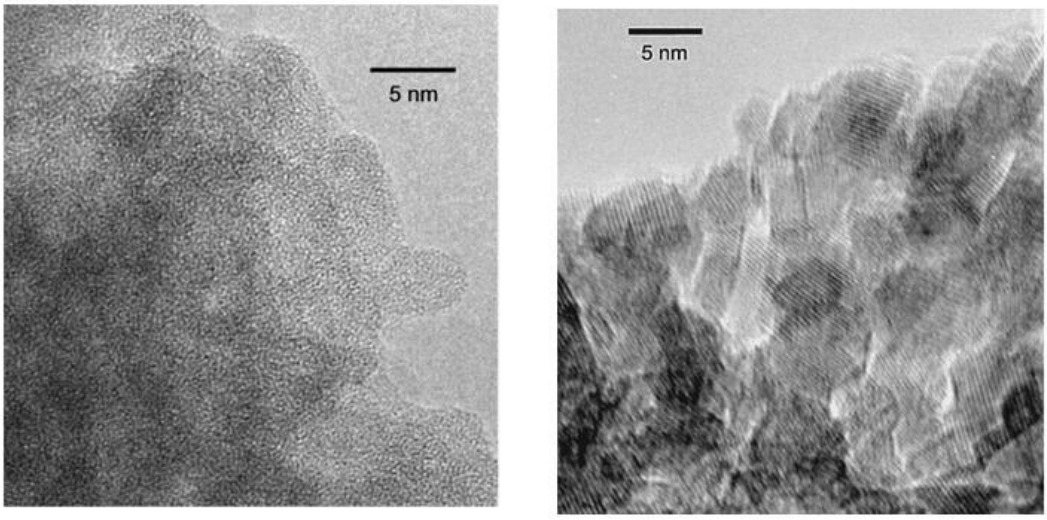

Figure 2: HR-TEM images of SZT (left hand) and SZT_773_6h (right hand).

Catalyst	**mg SO_4^{2-} (g ZrO_2-TiO_2)$^{-1}$**
SZT	1.4
SZT_773_6h	1.1

Table 3: Sulphates concentration quantified by ion chromatography.

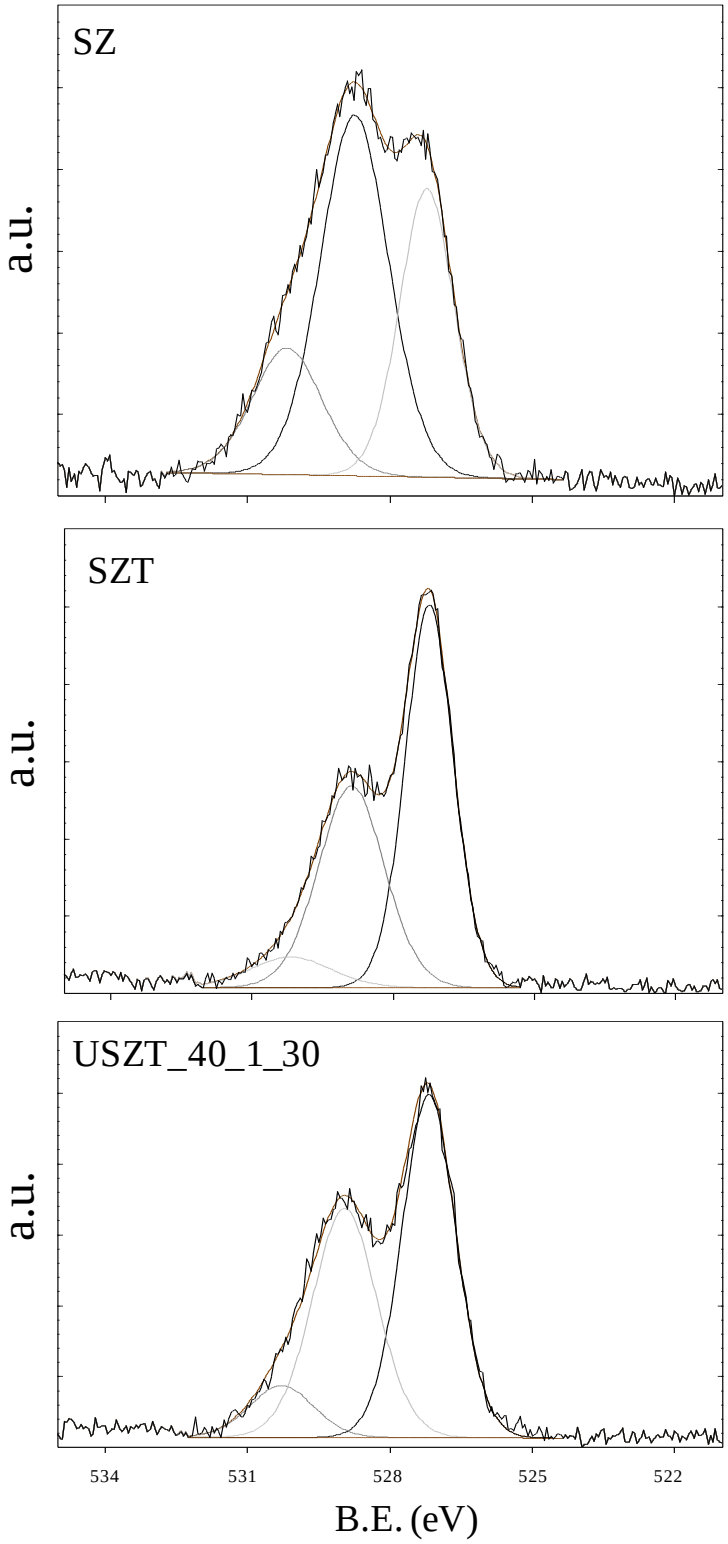

Figure 3: O 1s region of the samples SZ, SZT and USZT_40_1_30.

Sample	O 1s B.E. (eV)	Ti $2p_{3/2}$ B.E. (eV)	Zr $3d_{5/2}$ B.E. (eV)	S 2p B.E. (eV)	O/(Zr+Ti)	S/(Zr+Ti)	O/S
SZ	531.3	-	182.2	168.3	5.56	0.32	17.6
SZT	530.4	458.4	182.2	168.3	4.58	0.40	11.5
USZT_40_1_30	530.3	458.3	182.2	169.3	4.41	0.54	8.18

Table 4. XPS binding energies (B.E.) and elemental atomic ratios of the samples SZ, SZT and USZT_40_1_30.

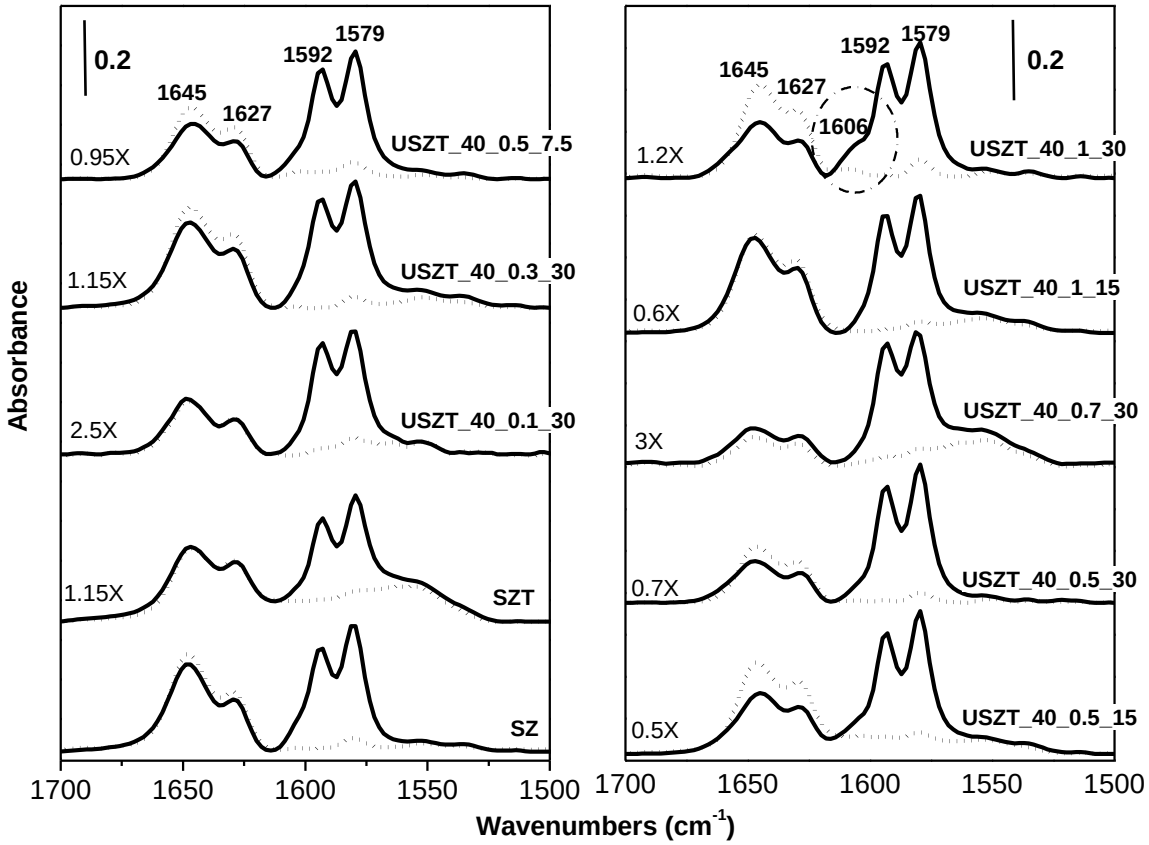

Figure 4: Differential absorbance spectra, normalized against the background spectrum of the starting sample activated at 623 K, relative to the adsorption/desorption of 2,6-DMP on some samples, as obtained in the vibrational region of 2,6-DMP 8a and 8b modes after contact at BT with the vapour pressure of 2,6-DMP (~2 Torr) [solid curves], and after BT evacuation of the 2,6-DMP excess [broken curves]. For a better comparison among spectra of the different systems, the different spectral sets have been ordinate-magnified, as indicated on the curves.

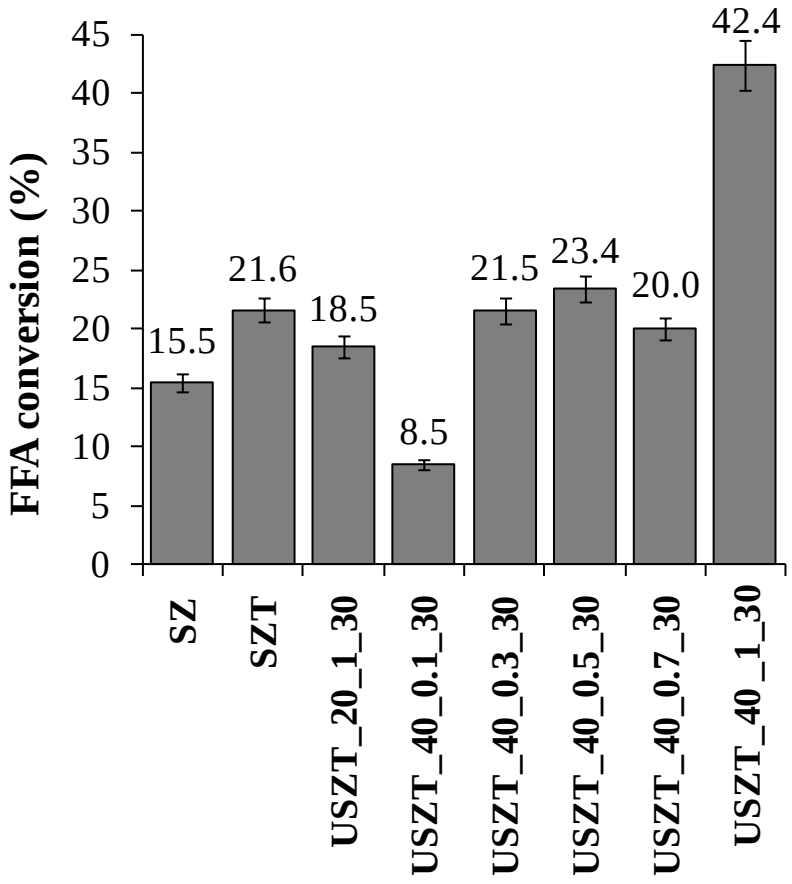

Figure 5: Conversions obtained for some of the samples synthesized using the same H_2O/precursors ratio in the FFA esterification reaction after 6 hour of reaction, 336 ± 2 K, slurry reactor, initial acidity: 7.5% wt (oleic acid), MeOH: oil=16:100$_{wt}$, catalyst: oleic acid=5:100$_{wt}$.

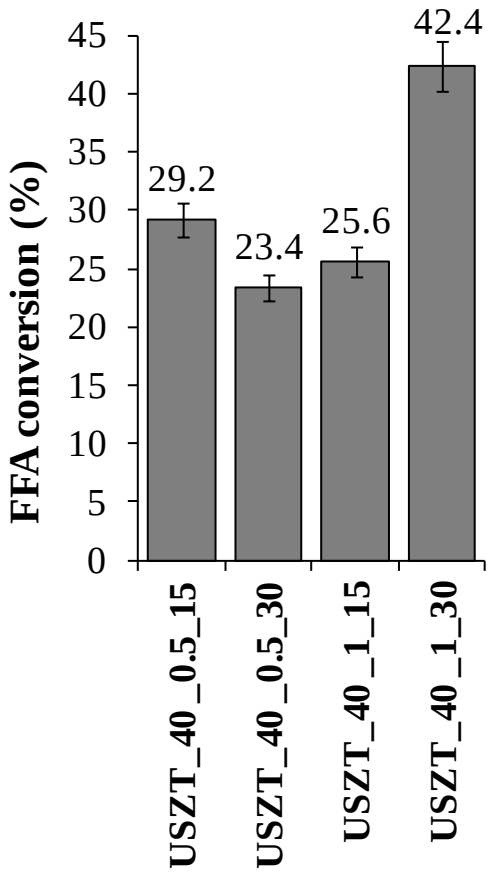

Figure 6: Conversions obtained for some of the samples synthesized using different H_2O/precursors ratio in the FFA esterification reaction after 6 hour of reaction, 336 ± 2 K, slurry reactor, initial acidity: 7.5% wt (oleic acid), MeOH: oil=16:100$_{wt}$, catalyst: oleic acid=5:100$_{wt}$.

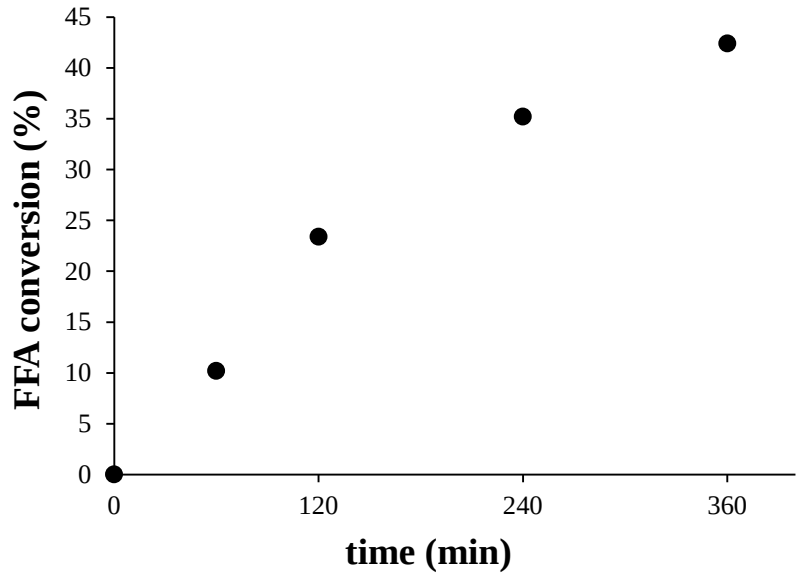

Figure 7: Example of a typical trend of FFA conversion, catalyst: USZT_40_1_30, 336 ± 2 K, slurry reactor, initial acidity: 7.5% wt (oleic acid), MeOH: oil=16:100_{wt}, catalyst: oleic acid=5:100_{wt}.

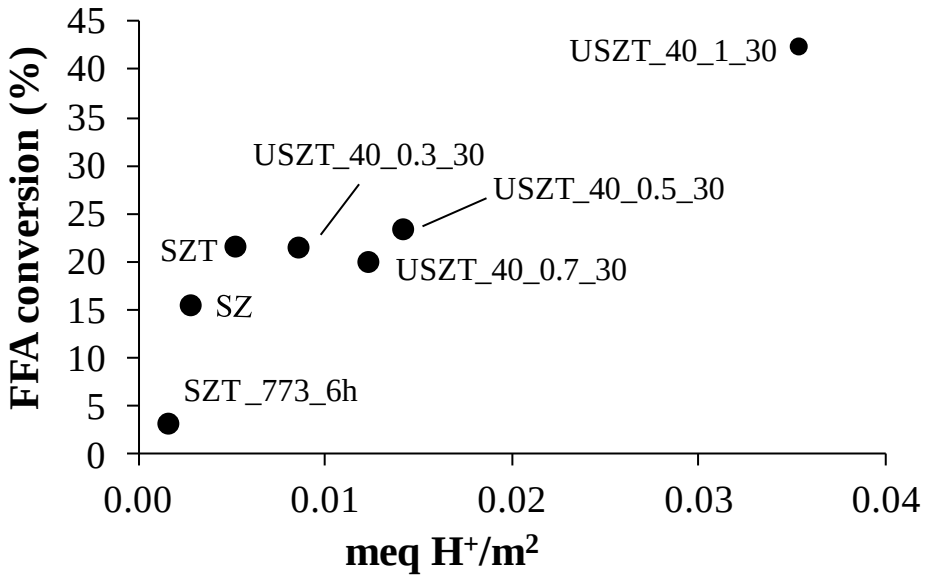

Figure 8: FFA conversion obtained for the different catalysts as a function of the concentration of the acid sites normalized to the surface area.